Supplementary Material for: Immuno-epidemiological life-history and the dynamics of SARS-CoV-2 over the next five years

Chadi M. Saad-Roy,[1*] Caroline E. Wagner,[2,3*]
Rachel E. Baker,[2,3] Sinead E. Morris,[4] Jeremy Farrar[5]
Andrea L. Graham,[2] Simon A. Levin,[2]
C. Jessica E. Metcalf,[2,6] Bryan T. Grenfell[2,6,7†]

[1]Lewis-Sigler Institute for Integrative Genomics,
Princeton University, Princeton NJ 08540, USA

[2]Department of Ecology and Evolutionary Biology,
Princeton University, Princeton NJ 08544, USA

[3]Princeton Environmental Institute,
Princeton University, Princeton NJ 08544, USA

[4]Department of Pathology and Cell Biology,
Columbia University Medical Center, New York NY 10032, USA

[5] The Wellcome Trust, London, UK

[6]Princeton School of Public and International Affairs,
Princeton University, Princeton NJ 08544, USA

[7]Fogarty International Center, National Institutes of Health, Bethesda MD 20892, USA,

[*]These authors contributed equally to this work

[†]To whom correspondence should be addressed; E-mail: grenfell@princeton.edu

S1 Methods

S1.1 Model description

We use the SIR(S) model from [1] depicted in Figure 1 of the main text, which assumes three immunity profiles (fully susceptible, S_P; partially immune, S_S; and fully immune, R) and two infection types (primary, I_P; and secondary, I_S), and allows for varying degrees of transmission (α) of and susceptibility (ϵ) to secondary relative to primary infections (where α and ϵ are assumed to lie between 0 and 1).

Individuals enter the fully susceptible class S_P at the birth rate ν, assumed to be equal to the death rate which, for non-fatal infections, is equivalent for all classes. Primary infections of fully susceptible individuals occur via contacts with individuals experiencing primary (I_P) or secondary (I_S) infections at rate $\beta(I_P + \alpha I_S)$, which accounts for the assumed reduction in the infectiousness of secondary infections relative to primary ones through the parameter α. The parameter β is the transmission rate, which in general is allowed to vary in time i.e. $\beta = \beta(t)$. Recovery from primary and secondary infections occurs at the same rate γ, at which point individuals enter the fully immune class R. Full immunity from natural infection is assumed to wane at rate δ, and individuals then become partially susceptible to infection. Secondary (and beyond) infections of partially susceptible individuals S_S once again occur through contacts with individuals experiencing primary or secondary infections at rate $\epsilon\beta(I_P + \alpha I_S)$, which accounts for the assumed reduction in susceptibility to secondary infections relative to primary ones through the parameter ϵ. These transitions between immunity and infection profiles define the following set of governing equations:

$$\frac{dS_P}{dt} = \mu - \beta(t)S_P(I_P + \alpha I_S) - \mu S_P, \tag{S1a}$$

$$\frac{dI_P}{dt} = \beta(t)S_P(I_P + \alpha I_S) - (\gamma + \mu)I_P, \tag{S1b}$$

$$\frac{dR}{dt} = \gamma(I_P + I_S) - \delta R - \mu R, \tag{S1c}$$

$$\frac{dS_S}{dt} = \delta R - \epsilon\beta(t)S_S(I_P + \alpha I_S) - \mu S_S, \tag{S1d}$$

$$\frac{dI_S}{dt} = \epsilon\beta(t)S_S(I_P + \alpha I_S) - (\gamma + \mu)I_S. \tag{S1e}$$

When a constant fraction ν of the fully and partially susceptible populations are vaccinated each week (thus entering the vaccinated class V), the governing equations are modified by the addition of the vaccination terms to become:

$$\frac{dS_P}{dt} = \mu - \beta(t)S_P(I_P + \alpha I_S) - \mu S_P - s_{\text{vax}}\nu S_P, \tag{S2a}$$
$$\frac{dI_P}{dt} = \beta(t)S_P(I_P + \alpha I_S) - (\gamma + \mu)I_P, \tag{S2b}$$
$$\frac{dR}{dt} = \gamma(I_P + I_S) - \delta R - \mu R, \tag{S2c}$$
$$\frac{dS_S}{dt} = \delta R + \delta_{\text{vax}}V - \epsilon\beta(t)S_S(I_P + \alpha I_S) - \mu S_S - s_{\text{vax}}\nu S_S, \tag{S2d}$$
$$\frac{dI_S}{dt} = \epsilon\beta(t)S_S(I_P + \alpha I_S) - (\gamma + \mu)I_S, \tag{S2e}$$
$$\frac{dV}{dt} = s_{\text{vax}}\nu(S_P + S_S) - (\delta_{\text{vax}} + \mu)V. \tag{S2f}$$

Individuals are assumed to lose vaccinal immunity at the rate δ_{vax}, at which point they enter the partially susceptible class. As for primary infections, all infections subsequent to vaccination are considered secondary and treated equivalently. Finally, the term s_{vax} is a switch that follows

$$s_{\text{vax}} = \begin{cases} 0 & t < t_{\text{vax}} \\ 1 & t \geq t_{\text{vax}}, \end{cases}$$

where t_{vax} is the time at which vaccination is introduced.

For all simulations, we take $\mu = 0.02\text{y}^{-1}$ corresponding to a yearly crude birth rate of 20 per 1000 people. Additionally, we take the infectious period to be $1/\gamma = 5$ days, consistent with the modeling in [2, 3] and the estimation of a serial interval of 5.1 days for Covid-19 in [4]. For the initial conditions of all simulations, we take $I_P = 1 \times 10^{-9}$ and assume the remainder of the population is in the fully susceptible class. The values of ϵ, α, δ, ν, t_{vax}, and δ_{vax} used in the various simulations are specified throughout the text.

S1.2 Determination of climatically-driven reproduction numbers

Seasonal values for R_0 enter the model via the transmission rate $\beta(t)$ calculated as:

$$\beta(t) = \gamma R_0(t). \tag{S3}$$

These values for R_0 are based on [3] and determined by:

$$R_0(t) = \exp(a * q(t) + log(R_{0max} - R_{0min})) + R_{0min} \tag{S4}$$

where $q(t)$ is specific humidity, a is the climate dependence parameter (set at -227.5) based on model fits for the HKU1 betacoronavirus taken from [3], and R_{0max}, R_{0min} are the maximum

and minimum reproductive numbers respectively, set at 2.5 and 1.5 reflecting estimated values for SARS-CoV-2 [3, 2] (see Section S2). Specific humidity comes from NASA's Modern-Era Retrospective analysis for Research and Applications version 2 (MERRA-2) dataset [5] and is based on an average thirty-year climatology. Latitude and longitude values are used to assign average specific humidity values from the nearest land-based MERRA gridcell to city locations.

S1.3 Definition of secondary peaks

The R software [6] peak finding algorithm `findpeaks` was used to identify peaks in the time series of total infections ($I = I_P + I_S$) for a minimum peak height of $I = 0.01$, i.e. 1% of the population infected. Spurious peaks arising from small oscillations when seasonal transmission rates permitted continuous population infection were eliminated by requiring that the value of I at the peak exceed the value of I at the start of the peak by at least 1×10^{-4}. Subsequent to this procedure, if more than one identified peak remained, the time between the earliest two peaks was selected as the time to the secondary peak, and the value of I during the second peak was selected as the magnitude of the secondary peak. If only one identified peak remained, it was determined that there was no secondary peak.

S1.4 Definition of clinically severe cases

We define the fraction of the population with severe disease as

$$I_{\text{sev}} = x_{\text{sev},p} I_P + x_{\text{sev},s} I_S, \tag{S5}$$

where $x_{\text{sev},p}$ and $x_{\text{sev},s}$ are the fractions of severe primary and secondary infections, respectively. The former can be estimated as $x_{\text{sev},p} = 0.14$ based on a case series report published by the Chinese Center for Disease Control and Prevention [7], which is in reasonable agreement with the categorization as severe of 173 of 1099 (16%) patients hospitalized for Covid-19 in China as of January 29, 2020 for whom clinical symptoms and outcomes data were available [8]. In contrast, the fraction of severe secondary infections $x_{\text{sev},s}$ is presently unknown and will likely depend on the nature of the adaptive immune response to primary SARS-CoV-2 infections.

S1.5 Equilibrium infection burdens as a function of vaccination rate and strength of immune response

Assume that s_{vax} is eventually turned on (a vaccine is introduced) and remains so, and that $\alpha = 1$ and $0 \leq \epsilon \leq 1$. Then let $I_T = I_P + I_S$ and consider the following system:

$$\frac{dI_T}{dt} = \beta I_T(S_P + \epsilon S_S) - (\gamma + \mu)I_T \tag{S6a}$$
$$\frac{dS_P}{dt} = \mu - \beta I_T S_P - (\mu + \nu)S_P \tag{S6b}$$
$$\frac{dS_S}{dt} = \delta R + \delta_{\text{vax}} V - \varepsilon\beta I_T S_S - (\mu + \nu)S_S \tag{S6c}$$
$$\frac{dR}{dt} = \gamma I_T - (\delta + \mu)R \tag{S6d}$$
$$\frac{dV}{dt} = \nu(S_P + S_S) - (\delta_{\text{vax}} + \mu)V. \tag{S6e}$$

Note that the I_S and I_P equations decouple from this system, and so their behaviours follow from the behaviours of S_P, I_T, and S_S. At a non-disease-free equilibrium ($I_T > 0$) it follows that

$$V^* = \frac{\nu}{\delta_{\text{vax}} + \mu}(S_P^* + S_S^*) \tag{S7a}$$
$$R^* = \frac{\gamma}{\delta + \mu} I_T^* \tag{S7b}$$
$$S_P^* = \frac{\mu}{\beta I_T^* + \mu + \nu} \tag{S7c}$$
$$\epsilon\beta I_T^* S_S^* + (\mu + \nu)S_S^* = \frac{\delta\gamma}{\delta + \mu} I_T^* + \frac{\delta_{\text{vax}}}{\delta_{\text{vax}} + \mu}\nu(S_P^* + S_S^*) \tag{S7d}$$

So that

$$S_S^* = \frac{\frac{\delta\gamma}{\delta+\mu} I_T^* + \frac{\nu\delta_{\text{vax}}}{\delta_{\text{vax}}+\mu}\left(\frac{\mu}{\beta I_T^* + \mu + \nu}\right)}{\epsilon\beta I_T^* + \mu + \nu - \frac{\delta_{\text{vax}}\nu}{\delta_{\text{vax}}+\mu}} \tag{S8}$$

Letting $Q = \frac{\beta}{\gamma+\mu}$, then $S_P^* + \epsilon S_S^* = \frac{1}{Q}$ at equilibrium. For simplification, we let

$$S_P^* = \frac{C}{DI_T^* + E}, \quad S_S^* = \frac{AI_T^* + B\frac{C}{DI_T^*+E}}{GI_T^* + H}, \tag{S9}$$

so that

$$\frac{C}{DI_T^* + E} + \epsilon\frac{AI_T^* + B\frac{C}{DI_T^*+E}}{GI_T^* + H} = \frac{1}{Q}. \tag{S10}$$

Multiplying both sides by $(GI_T^* + H)(DI_T^* + E)$ gives

$$C(GI_T^* + H) + \epsilon AI_T^*(DI_T^* + E) + \epsilon BC = \frac{1}{Q}(GI_T^* + H)(DI_T^* + E), \tag{S11}$$

so that subtracting the LHS on both sides gives $f(I_T^*) = MI_T^{*^2} + NI_T^* + P = 0$, where

$$M = \epsilon AD - \frac{GD}{Q} \tag{S12a}$$

$$N = GC + \epsilon AE - \frac{GE}{Q} - \frac{DH}{Q} \tag{S12b}$$

$$P = CH + \epsilon BC - \frac{HE}{Q} \tag{S12c}$$

where $A = \frac{\delta\gamma}{\delta+\mu}$, $B = \frac{\delta_{\text{vax}}\nu}{\delta_{\text{vax}}+\mu}$, $C = \mu$, $D = \beta$, $E = \mu + \nu$, $G = \epsilon\beta$, $H = \mu + \nu - \frac{\delta_{\text{vax}}\nu}{\delta_{\text{vax}}+\mu}$.

Next, we show that if the associated $\mathcal{R}_0 > 1$, then there is a unique positive root that lies between 0 and 1. Otherwise, if $\mathcal{R}_0 < 1$, there is no positive root.

Substituting A, D, G, D, Q into M gives that

$$M = \epsilon\beta\mu\left(-\frac{\gamma}{\delta+\mu} - 1\right) < 0. \tag{S13}$$

At the disease-free equilibrium, $R^{(0)} = I_T^{(0)} = 0$, and it can be shown that $S_P^{(0)} = \frac{\mu}{\mu+\nu}$, and $S_S^{(0)} = \frac{\nu}{\nu+\mu}\frac{\delta_{\text{vax}}}{\mu+\nu+\delta_{\text{vax}}}$. Thus, the basic reproduction number of this system is

$$\mathcal{R}_0 = \frac{\beta}{\gamma+\mu}\left(\frac{\mu}{\mu+\nu} + \epsilon\frac{\nu}{\nu+\mu}\frac{\delta\text{vax}}{\mu+\nu+\delta_{\text{vax}}}\right). \tag{S14}$$

If $I_T > 0$ and small, and $\mathcal{R}_0 < 1$, then $\frac{dI_T}{dt} < 0$ and the disease dies out, i.e. the disease-free equilibrium is locally stable if $\mathcal{R}_0 < 1$. On the other hand, if $\mathcal{R}_0 > 1$ and I_T is small, then $\frac{dI_T}{dt} > 0$.

Substituting the values of C, H, B, C, E, Q in P gives that

$$P = \mu(\mu+\nu)\left(\frac{\delta_{\text{vax}}+\mu+\nu}{\delta_{\text{vax}}+\mu}\right)\left(\frac{\gamma+\mu}{\beta}\right)(\mathcal{R}_0 - 1). \tag{S15}$$

Thus, $P > 0$ if and only if $\mathcal{R}_0 > 1$.

Since $M < 0$, and $P > 0$ if and only $\mathcal{R}_0 > 1$, then by Descartes' Rule of Signs, $f(I_T^*)$ has exactly one positive real root if $\mathcal{R}_0 > 1$. Further, since $f(0) > 0$ and $f(1) < 0$ this positive root lies between 0 and 1. Therefore, there is a unique endemic equilibrium if $\mathcal{R}_0 > 1$.

For $\mathcal{R}_0 < 1$, it can be shown using Equations (S12b) and (S14) that $N < 0$, and so with $P < 0$ and $M < 0$, this guarantees that $f(I_T^*)$ has no positive root when $\mathcal{R}_0 < 1$ and so no subthreshold equilibrium exists when $\mathcal{R}_0 < 1$.

S1.6 Minimal vaccination rate for $\mathcal{R}_0 < 1$

Finally, we find the vaccination rate $\nu_{\min}$ so that $\mathcal{R}_0 = 1$, and so for $\nu > \nu_{\min}$ then $\mathcal{R}_0 < 1$. Thus, we solve $\mathcal{R}_0 = 1$ for ν. Letting $a_1 = \frac{\beta}{\gamma+\mu}$, $a_2 = \mu$, $a_3 = \epsilon\delta_{\text{vax}}$, and $a_4 = \mu + \delta_{\text{vax}}$. Then,

$$1 = \frac{a_1}{a_2 + \nu_{\min}} \left(a_2 + \frac{a_3 \nu_{\min}}{a_4 + \nu_{\min}} \right). \tag{S16}$$

Rearranging the above equation gives

$$0 = \nu_{\min}^2 + \nu_{\min} \left(a_2 + a_4 - a_1 a_2 - a_1 a_3 \right) + a_2 a_4 - a_1 a_2 a_4 = \nu_{\min}^2 + b_1 \nu_{\min} - b_0 = g(\nu_{\min}). \tag{S17}$$

Note that $b_0 = a_2 a_4 (a_1 - 1)$. For $\nu > 0$, then $\frac{\beta}{\gamma+\mu} > \mathcal{R}_0$. (cf. Eq. S14). Since $a_1 = \frac{\beta}{\gamma+\mu} > 1$, then $b_0 > 0$ if $\mathcal{R}_0 > 1$. Thus, the positive root of $g(\nu_{\min})$ is

$$\nu_{\min} = \frac{-b_1 + \sqrt{b_1^2 + 4b_0}}{2}. \tag{S18}$$

Note that for $a_1 = \frac{\beta}{\gamma+\mu} = 1$ (i.e. the reproduction number for fully immunizing infections $\epsilon = 0$), $\nu_{\min} = 0$. To gain further intuition, assume that a_1 is close to 1, i.e. $a_1 = 1 + w$, for $w > 0$ and small, which implies $\nu_{\min}$ is small. Then, neglecting higher order terms in $\nu_{\min}$, the linearization of Equation (S17) gives

$$\nu_{\min} = \frac{b_0}{b_1},$$

which for small w, simplifies to

$$\nu_{\min} = \frac{a_2 a_4}{a_4 - a_3} w.$$

Substituting in the values of a_2, a_3, and a_4, and dividing by a_4, we then obtain the following linear approximation for $\nu_{\min}$:

$$\nu_{\min} = \frac{\mu}{1 - \frac{\epsilon\delta_{\text{vax}}}{\mu + \delta_{\text{vax}}}} w.$$

S2 Caveats

Our model explores the impact of the strength and duration of individual immunity on the epidemic dynamics of Covid-19, accounting for seasonally- and NPI-induced changes in transmission rates as well as a simplified vaccination scenario. However, to reduce the complexity of our framework and focus on key determinants, we have made a number of simplifying assumptions.

- First, we assume exponential waiting times for immune duration, and that tertiary (and beyond) infections are equivalent to secondary infections due to the relatively short timescales that we examined. However, repeated subsequent viral exposures may heighten adaptive immune responses and thus lead to stronger and longer immunity. With increases in infection, viral evolution and immune escape could also alter immunity landscapes. Extending our framework to address these nuances would aid in characterizing longer-term endemic dynamics.

- Second, informed by phylogenetic relationships, we have assumed that climatic influences on SARS-CoV-2 transmission are very similar to the β–CoV HCoV-HKU1. With further data tying climate with transmission, more accurate seasonal variation could be incorporated.

- Third, we have assumed that social distancing scenarios result in a fixed reduction in the transmission rate for specific time periods. However, it is likely that reductions in β due to NPIs will vary over time due to changes in a number of factors including human behaviour. Further, NPIs may result in changes in contact patterns and hence non-uniform effects across age groups [9] and heterogeneities in populations can decrease the herd immunity threshold [10]. In our model, these could be investigated through the addition of age-structure, although here we follow [3] and [2] in assuming a well-mixed urban population. Additionally, the specific time periods during which the NPIs are assumed to be enforced in this work were designed to capture a variety of policy scenarios. In reality, the timing of NPIs will vary by location, and consequently the incorporation of spatial structure and stochasticity as well as these data as they become more readily available could be used to tailor model predictions.

- Fourth, we assume qualitatively uniform adaptive immune responses among individuals. However, it is increasingly being recognized that both T-cell- and antibody-mediated adaptive immune responses are associated with recovery from SARS-CoV-2 infection, possibly to different degrees among individuals. Similarly, vaccine efficacy may vary within groups owing to demographic, physiological, or environmental factors. Given that the strength and duration of immunity conferred by T and B cells may vary, an important area for future work will be to assume heterogeneities between individuals in adaptive immune responses after primary infection or vaccination.

- Fifth, the proportion of severe primary cases $x_{\text{sev,p}}$ assumed in this work from case series

reports may be an overestimation since these reports focus on confirmed or suspected cases of Covid-19 rather than total infections, although our qualitative predictions of epidemic dynamics should be robust to changes in the magnitude of this value. It is plausible, however, that the severity of secondary infections may be correlated with viral loads and hence the transmissibility of secondary infections, and therefore a direction for future work may be to incorporate within-host and cross-scale modeling frameworks (see for example [11]).

- Sixth, we have modelled a highly simplified vaccination scenario in which a constant proportion of the fully and partially susceptible populations are immunized weekly. However, our model results are qualitatively similar if other scenarios such as a more pulse-like campaign immunizing a larger portion of the population is implemented (see Figure S12), although without sustained immunization policies the possibility of waning vaccine immunity may result in less efficient outbreak control under this scenario. Models exploring immune and behavioural responses to multiple vaccine doses could be developed to address this. Further, in light of the severity of the current Covid-19 pandemic, it is likely that increases in the production and deployment capacity over time could lead to higher vaccination rates than our conservative estimate based on H1N1 data. As these processes are implemented, these group-dependent rates could be inferred from data and implemented into our model to refine our predictions. Nevertheless, in the early stages of vaccine deployment, limitations in supply may necessitate the prioritization of higher-risk groups (i.e. the elderly and health-care workers), and a meta-population approach that incorporates these complexities could be developed. Additionally, our simple model assumes that vaccines and primary infections confer the same degree of protection to secondary infection following immune waning (i.e. the reduction in susceptibility to secondary infection is ϵ for both), although more complex scenarios could be simulated in which this level of protection differs.

- Finally, asymptomatic transmission has been identified as an important driver of Covid-19 disease spread [12]. Although our findings are robust to moderate assumptions on the proportion of asymptomatic cases (results not shown), more refined models incorporating heterogeneity in primary infection could assess this effect more quantitatively.

In all cases, the relaxation of the assumptions made in the underlying model framework and the integration of additional complexities are important areas of future work to properly predict the course of SARS-CoV-2 infections in a post-pandemic world.

S3 Supplementary Figures and Results

S3.1 Schematic of possible population-level immune responses to SARS-CoV-2 infection

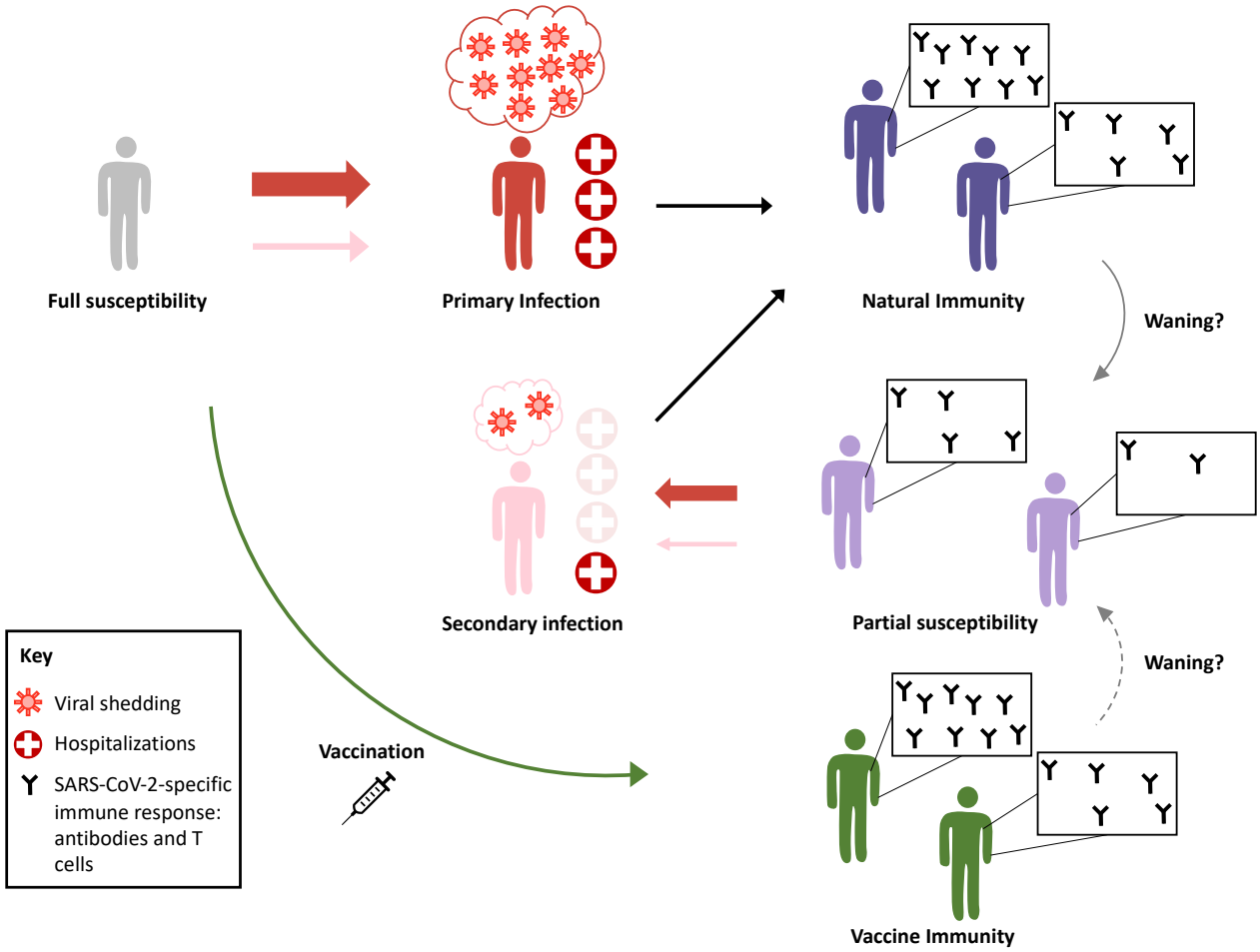

Figure S1: Schematic of possible population-level immune responses to SARS-CoV-2 infection. Fully susceptible individuals can experience a primary infection through contact with infectious individuals. Following infection, individuals may acquire varying levels of natural immunity, denoted by the presence of SARS-CoV-2 specific immune responses such as antibodies and T cells. Over time, this natural immunity may wane, and individuals may be susceptible to secondary infections. Individuals experiencing primary infections may experience greater amounts of viral replication and shedding than individuals experiencing secondary infections, resulting in a greater contribution to the force infection (larger red arrows than pink arrows). Further, individuals with partial immunity may be less susceptible to secondary infections than fully susceptible individuals are to primary infections, as illustrated by the smaller red and pink arrows leading away from partially susceptible individuals compared to fully susceptible ones. Additionally, the proportion of severe cases requiring hospitalization in individuals experiencing secondary infections may be smaller than that for primary infections, as shown by the number of red crosses, but there are also possible scenarios where severity of secondary infections could exceed that of primary ones due to phenomena such as antibody-dependent enhancement, as shown by the faded-out crosses. Finally, the availability of a vaccine would provide immunity to fully susceptible individuals without requiring infection, although this immunity may also wane, possibly at a different rate than natural immunity.

S3.2 Time series of weekly reproduction numbers

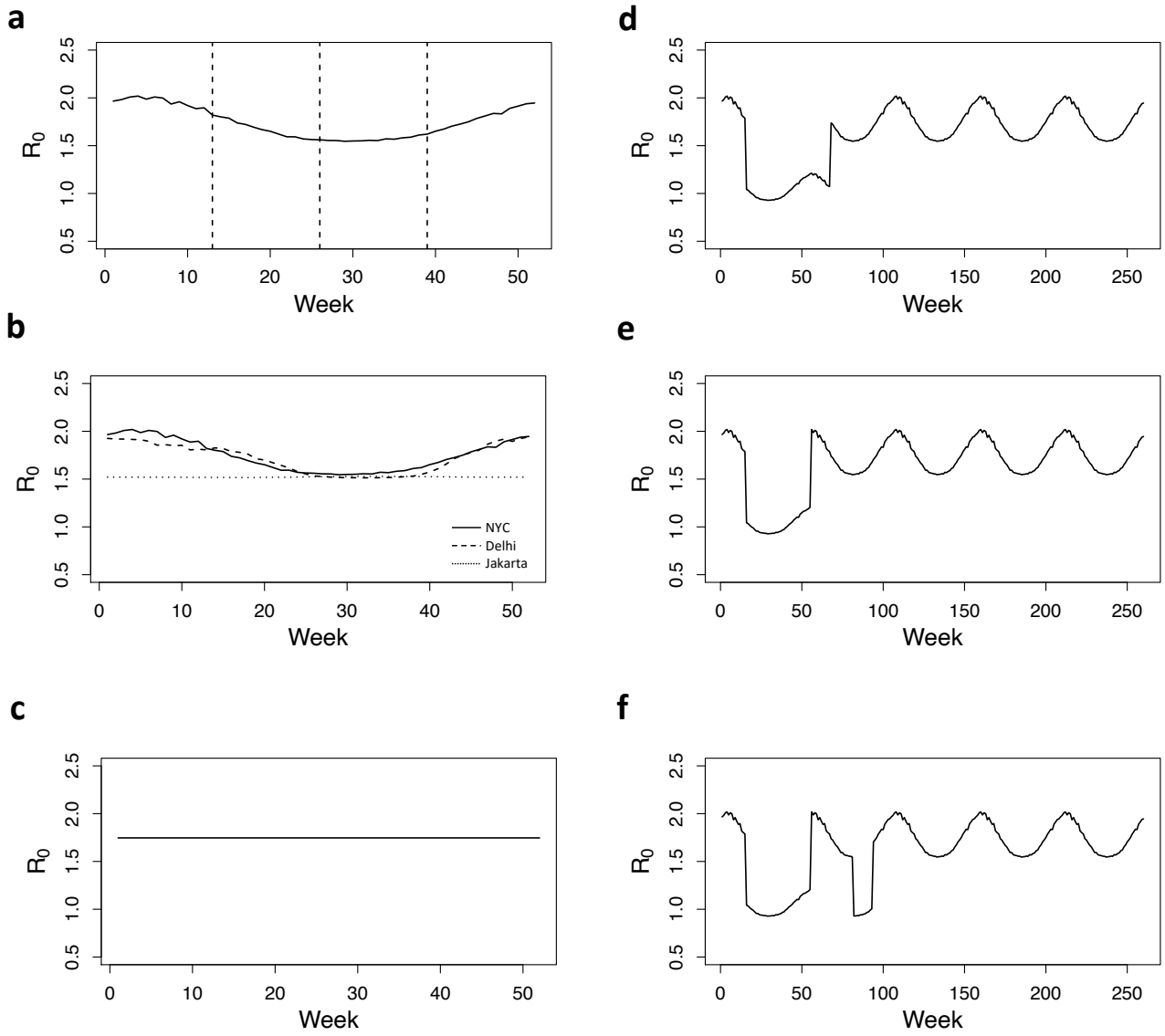

Figure S2: Weekly reproduction numbers for assuming seasonality derived from the climate of NYC. The lags in seasonality relative to the epidemic onset considered in Figures S3-S5 are indicated by the dashed black lines. (b) Seasonal weekly reproduction numbers derived from the climates of NYC (solid line), Delhi (dashed line), and Jakarta (dotted line). (c) Weekly reproduction numbers assuming no seasonality determined as the mean of the seasonal values in (a). The time series in (a)-(c) are repeated to achieve continuous five-year transmission rates in the epidemiological modeling. (d) and (e): weekly reproduction numbers with seasonality derived from the climate of NYC and social distancing resulting in a reduction in R_0 to 60% of its original value between weeks 16 and 55 (d), and between weeks 16 and 55 as well as weeks 82 and 93 (e).

S3.3 Effect of climate-driven seasonality on timing and magnitude of subsequent peaks

Recent work suggests that climate may play an important role in the timing of longer-term SARS-CoV-2 endemic cycles, although the dynamics of the pandemic stage are dominated by

the near complete population susceptibility at the time of the first case [3]. We find that transmission seasonality significantly modulates the dynamics of the second and subsequent epidemic peaks. In particular, seasonality drives non-monotonicity in the size and timing of the secondary peak as a function of either the duration of immunity or the reduction in susceptibility to secondary infections ϵ (Figures S3a and S3b). Thus, counter-intuitively, the size of the secondary peak can be larger under conditions when ϵ is smaller or immunity to SARS-CoV-2 has a longer duration due to the seasonal variation in the transmission rate and consequently the relative timing of susceptible accumulation (Figures S3c and S3d). These results are robust to initiating the epidemic at other points along the seasonal cycle (Figures S4-S6), and in locations with smaller annual fluctuations in climate (e.g. Delhi and Jakarta), this non-monotonic behaviour is increasingly suppressed (Figures S2b, S7, and S8). In the limit of a constant transmission rate, taken here to be derived from the mean value of these seasonal NYC-based weekly reproduction numbers ($\overline{R}_0 = 1.75$, see Methods and Figure S2c), secondary peaks are smaller in magnitude and occur later if susceptibility to secondary infection ϵ is reduced or if the duration of immunity is increased (see Figure S9 of the supplementary material). These dynamics are driven by a decrease in the number of infected individuals (and hence the force of infection) when ϵ is decreased and an increase in the proportion of partially and fully immune individuals for larger values of $1/\delta$. The trend is further amplified if secondary infections transmit less readily (i.e. $\alpha < 1$, Figure S10).

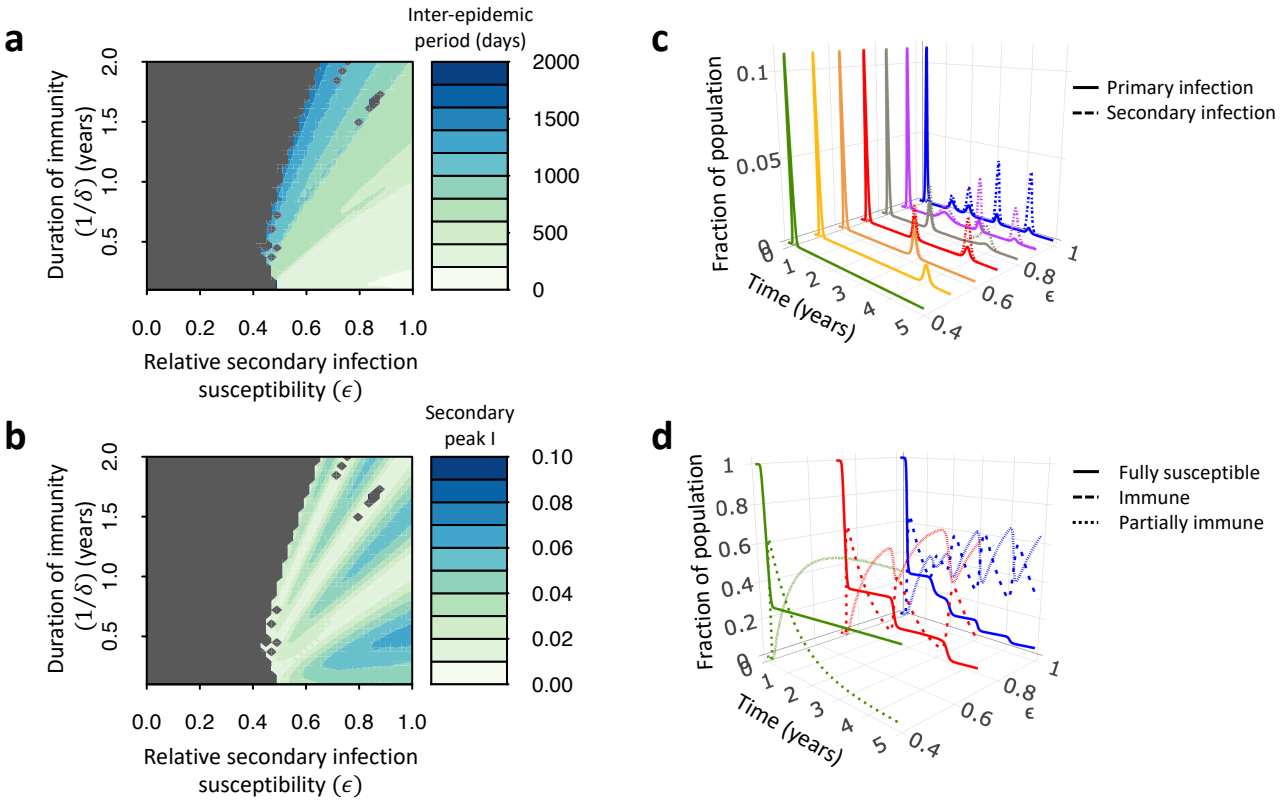

Figure S3: Effect of immunity length ($1/\delta$) and reduction in relative susceptibility to secondary infections (ϵ) on primary and secondary infection burden and timing when secondary infections are equally transmissible ($\alpha = 1$) with a seasonal transmission rate derived from the climate of NYC. In (a) the number of days between the first and second peak, and in (b) the total fraction of the population infected during the second peak are shown as a function of ϵ and $1/\delta$ with grey regions indicating no secondary peak satisfying the threshold size within a period of five years (see the Methods). In (c) the times series of primary (solid lines) and secondary (dashed lines) infections are shown for various values of ϵ and a duration of immunity of $1/\delta = 1$ year. In (d) the times series of the fully susceptible (S_P, solid lines), immune (R, dashed lines), and partially immune (S_S, dotted lines) populations are shown for various values of ϵ and a duration of immunity of $1/\delta = 1$ year.

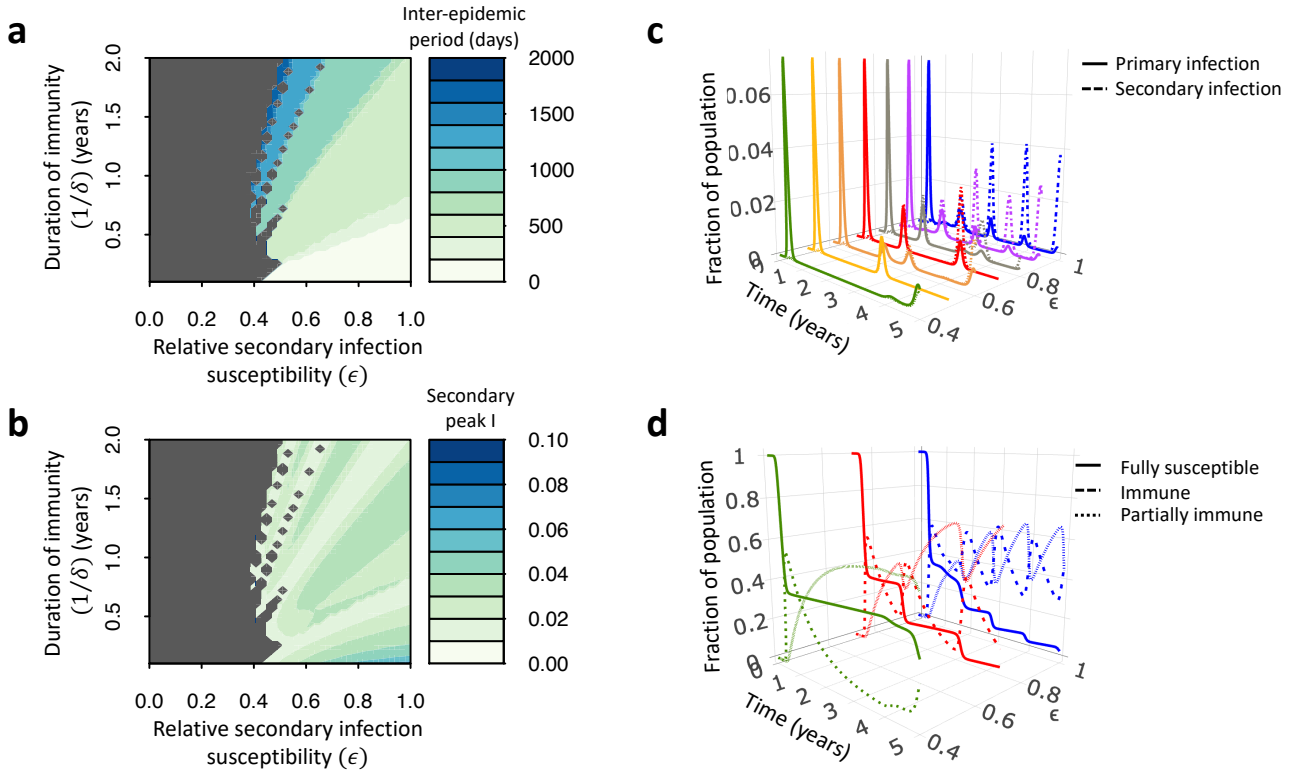

Figure S4: Effect of immunity length ($1/\delta$) and reduction in relative susceptibility to secondary infections (ϵ) on primary and secondary infection burden and timing when secondary infections are equally transmissible ($\alpha = 1$) with a seasonal transmission rate derived from the climate of NYC lagged 13 weeks. In (a) the number of days between the first and second peak, and in (b) the total fraction of the population infected during the second peak are shown as a function of ϵ and $1/\delta$ with grey regions indicating no secondary peak satisfying the threshold size within a period of five years (see the Methods). In (c) the times series of primary (solid lines) and secondary (dashed lines) infections are shown for various values of ϵ and a duration of immunity of $1/\delta = 1$ year. In (d) the times series of the fully susceptible (S_P, solid lines), immune (R, dashed lines), and partially immune (S_S, dotted lines) populations are shown for various values of ϵ and a duration of immunity of $1/\delta = 1$ year.

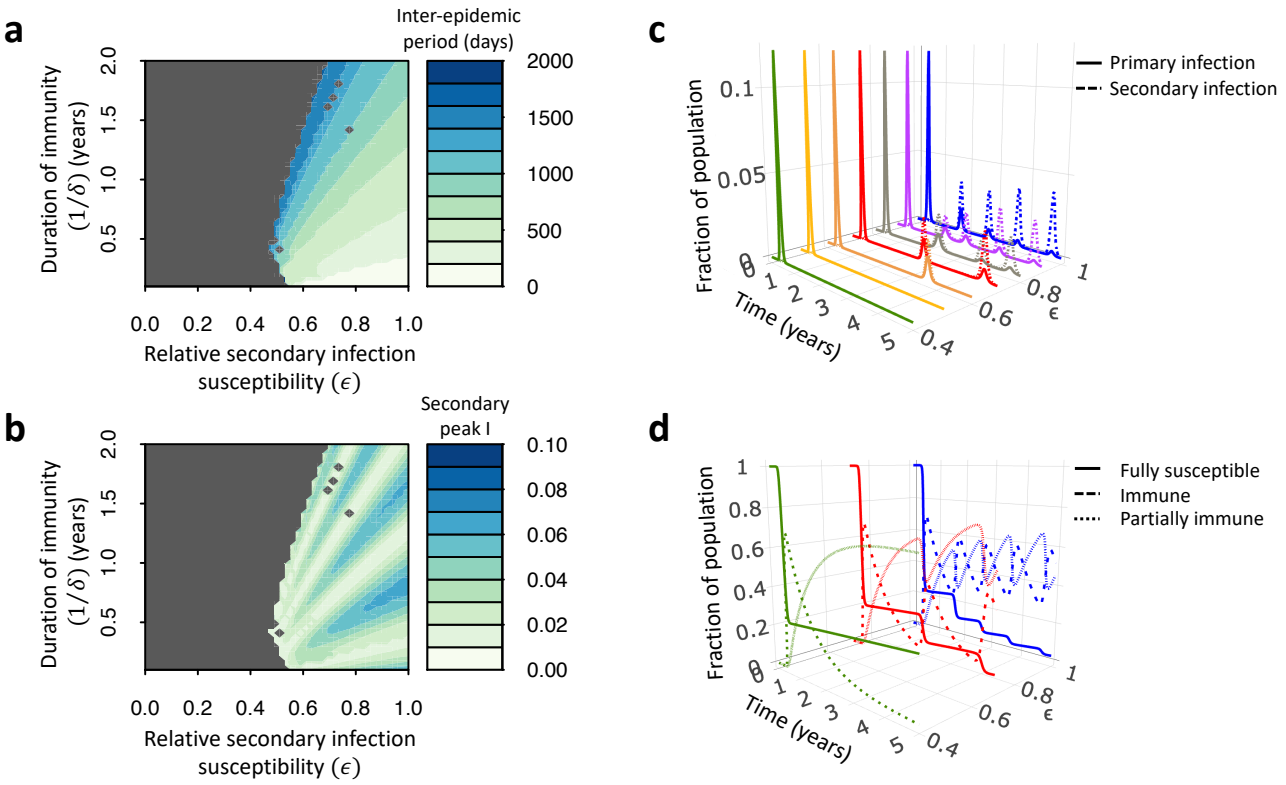

Figure S5: Effect of immunity length ($1/\delta$) and reduction in relative susceptibility to secondary infections (ϵ) on primary and secondary infection burden and timing when secondary infections are equally transmissible ($\alpha = 1$) with a seasonal transmission rate derived from the climate of NYC lagged 26 weeks. In (a) the number of days between the first and second peak, and in (b) the total fraction of the population infected during the second peak are shown as a function of ϵ and $1/\delta$ with grey regions indicating no secondary peak satisfying the threshold size within a period of five years (see the Methods). In (c) the times series of primary (solid lines) and secondary (dashed lines) infections are shown for various values of ϵ and a duration of immunity of $1/\delta = 1$ year. In (d) the times series of the fully susceptible (S_P, solid lines), immune (R, dashed lines), and partially immune (S_S, dotted lines) populations are shown for various values of ϵ and a duration of immunity of $1/\delta = 1$ year.

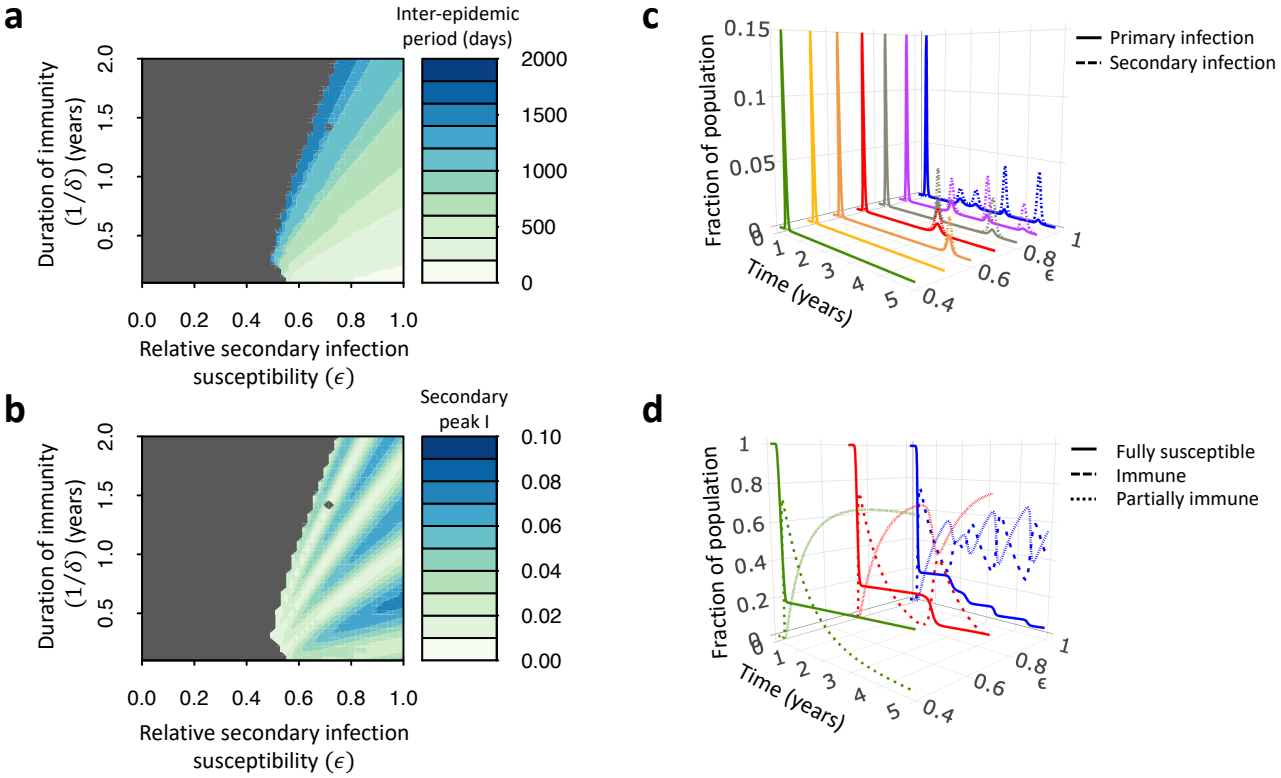

Figure S6: Effect of immunity length ($1/\delta$) and reduction in relative susceptibility to secondary infections (ϵ) on primary and secondary infection burden and timing when secondary infections are equally transmissible ($\alpha = 1$) with a seasonal transmission rate derived from the climate of NYC lagged 39 weeks. In (a) the number of days between the first and second peak, and in (b) the total fraction of the population infected during the second peak are shown as a function of ϵ and $1/\delta$ with grey regions indicating no secondary peak satisfying the threshold size within a period of five years (see the Methods). In (c) the times series of primary (solid lines) and secondary (dashed lines) infections are shown for various values of ϵ and a duration of immunity of $1/\delta = 1$ year. In (d) the times series of the fully susceptible (S_P, solid lines), immune (R, dashed lines), and partially immune (S_S, dotted lines) populations are shown for various values of ϵ and a duration of immunity of $1/\delta = 1$ year.

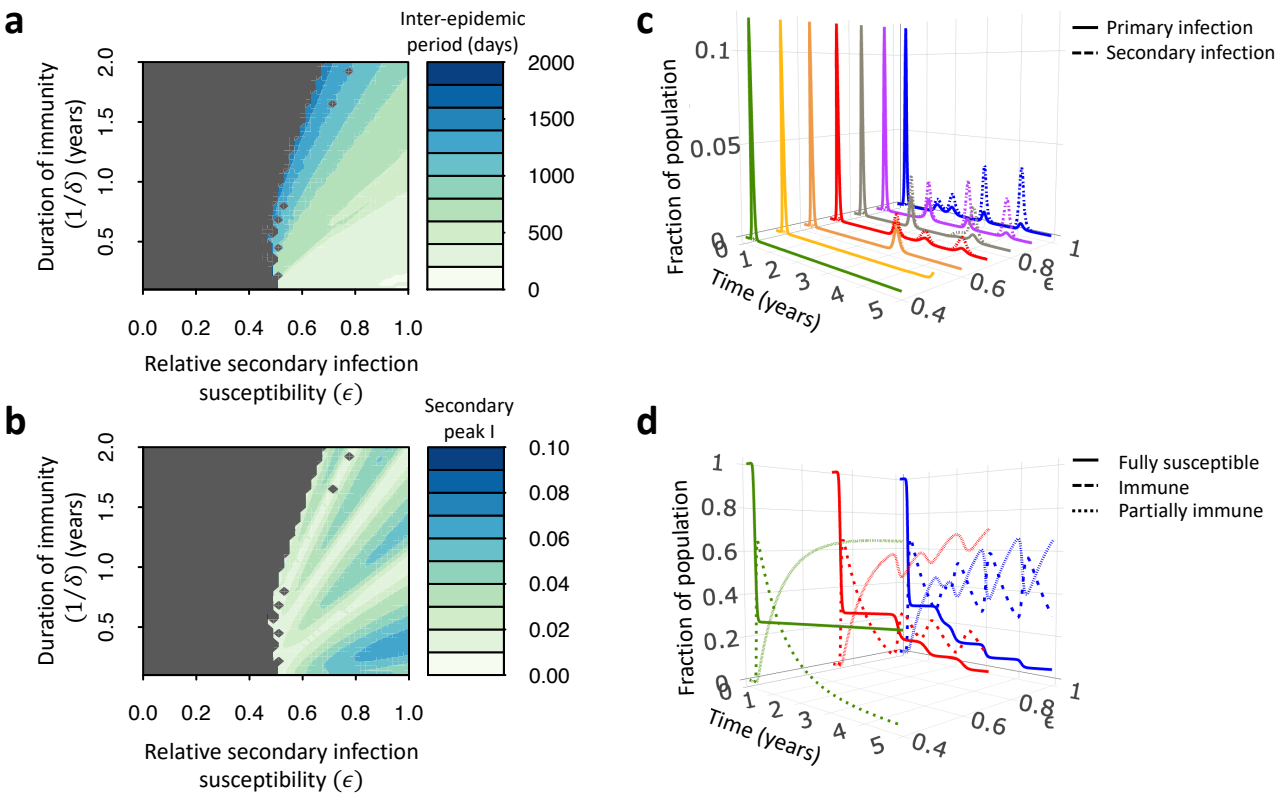

Figure S7: Effect of immunity length ($1/\delta$) and reduction in relative susceptibility to secondary infections (ϵ) on primary and secondary infection burden and timing when secondary infections are equally transmissible ($\alpha = 1$) with a seasonal transmission rate derived from the climate of Delhi. The weekly reproduction numbers used are those plotted in Figure S2b. In (a) the number of days between the first and second peak, and in (b) the total fraction of the population infected during the second peak are shown as a function of ϵ and $1/\delta$ with grey regions indicating no secondary peak satisfying the threshold size within a period of five years (see the Methods). In (c) the times series of primary (solid lines) and secondary (dashed lines) infections are shown for various values of ϵ and a duration of immunity of $1/\delta = 1$ year. In (d) the times series of the fully susceptible (S_P, solid lines), immune (R, dashed lines), and partially immune (S_S, dotted lines) populations are shown for various values of ϵ and a duration of immunity of $1/\delta = 1$ year.

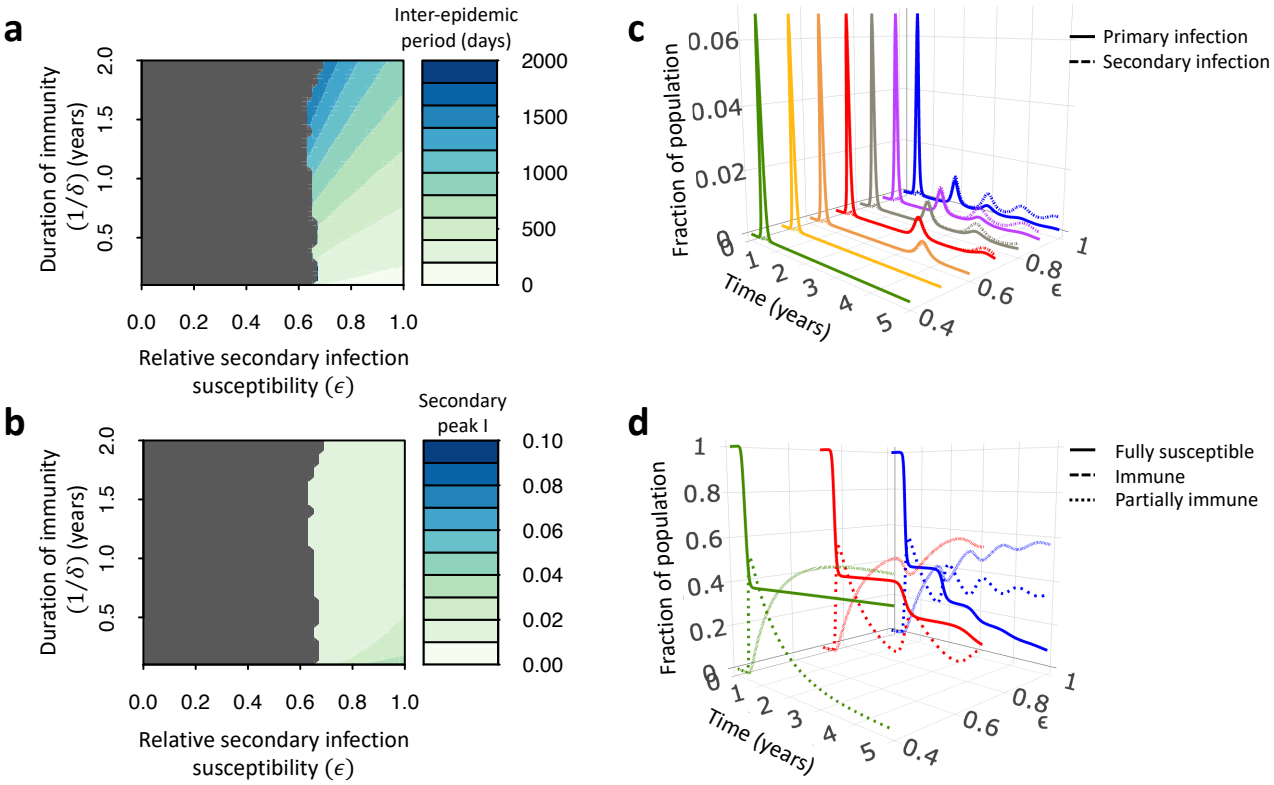

Figure S8: Effect of immunity length ($1/\delta$) and reduction in relative susceptibility to secondary infections (ϵ) on primary and secondary infection burden and timing when secondary infections are equally transmissible ($\alpha = 1$) with a seasonal transmission rate derived from the climate of Jakarta. The weekly reproduction numbers used are those plotted in Figure S2b. In (a) the number of days between the first and second peak, and in (b) the total fraction of the population infected during the second peak are shown as a function of ϵ and $1/\delta$ with grey regions indicating no secondary peak satisfying the threshold size within a period of five years (see the Methods). In (c) the times series of primary (solid lines) and secondary (dashed lines) infections are shown for various values of ϵ and a duration of immunity of $1/\delta = 1$ year. In (d) the times series of the fully susceptible (S_P, solid lines), immune (R, dashed lines), and partially immune (S_S, dotted lines) populations are shown for various values of ϵ and a duration of immunity of $1/\delta = 1$ year.

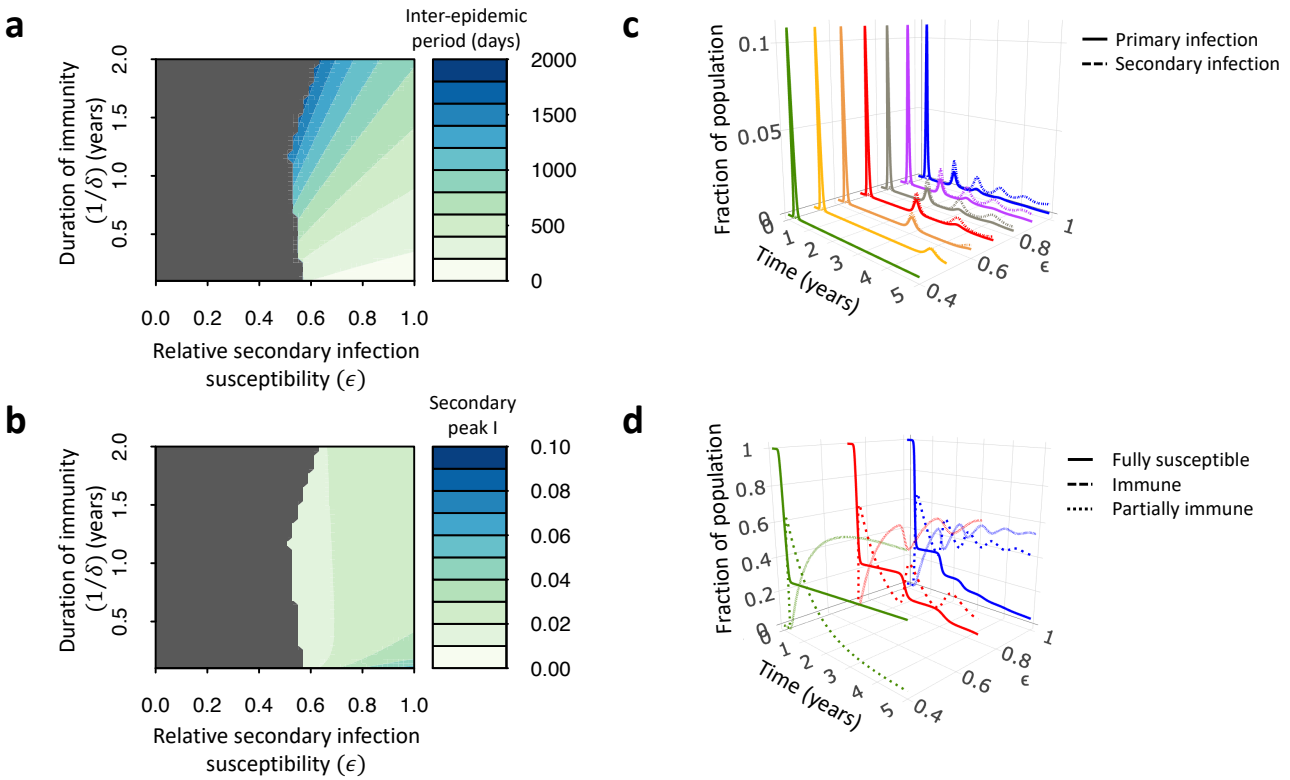

Figure S9: Effect of immunity length ($1/\delta$) and reduction in relative susceptibility to secondary infections (ϵ) on primary and secondary infection burden and timing when secondary infections are equally transmissible ($\alpha = 1$) and the transmission rate is constant (as plotted in Figure S2c). In (a) the number of days between the first and second peak, and in (b) the total fraction of the population infected during the second peak are shown as a function of ϵ and $1/\delta$ with grey regions indicating no secondary peak satisfying the threshold size within a period of five years (see the Methods). In (c) the times series of primary (solid lines) and secondary (dashed lines) infections are shown for various values of ϵ and a duration of immunity of $1/\delta = 1$ year. In (d) the times series of the fully susceptible (S_P, solid lines), immune (R, dashed lines), and partially immune (S_S, dotted lines) populations are shown for various values of ϵ and a duration of immunity of $1/\delta = 1$ year.

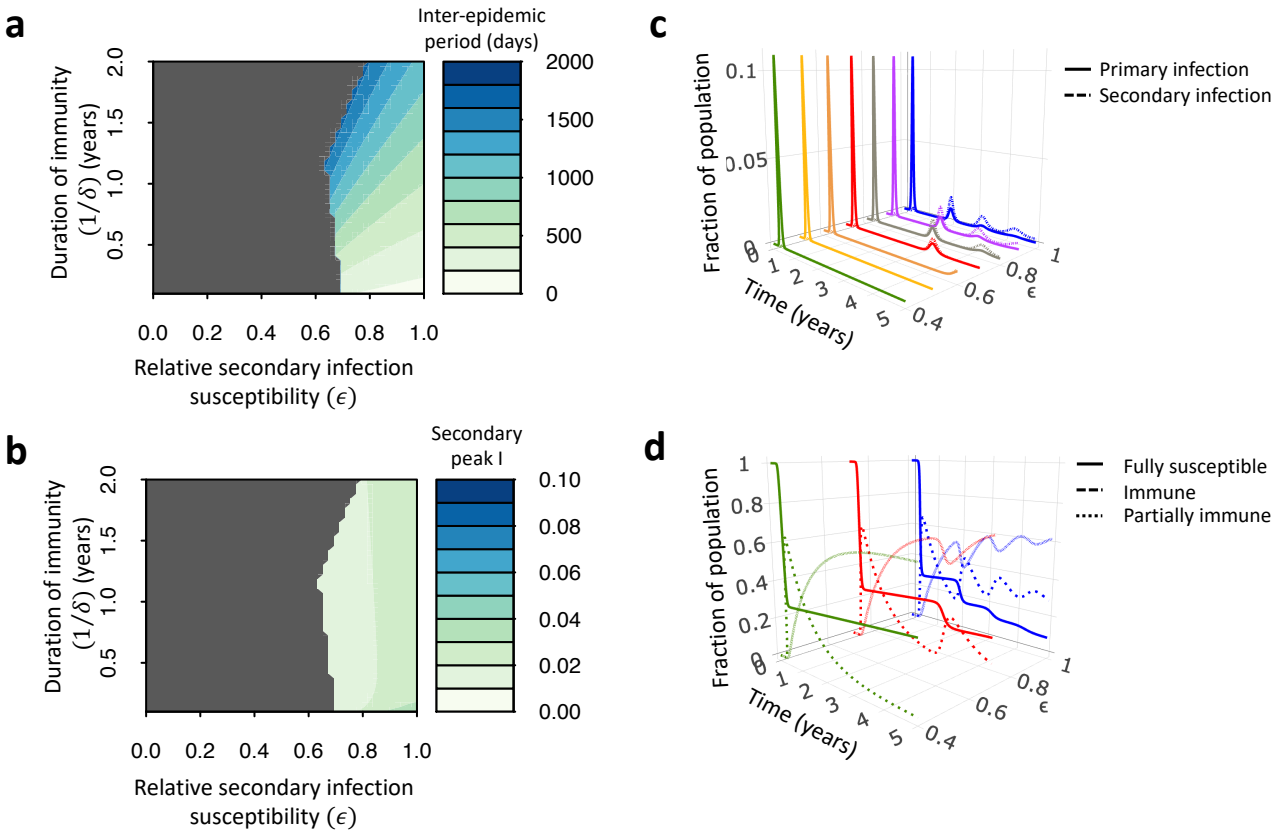

Figure S10: Effect of immunity length ($1/\delta$) and reduction in relative susceptibility to secondary infections (ϵ) on primary and secondary infection burden and timing when secondary infections are relatively less transmissible ($\alpha = 0.8$) and the transmission rate is constant (as plotted in Figure S2c). In (a) the number of days between the first and second peak, and in (b) the total fraction of the population infected during the second peak are shown as a function of ϵ and $1/\delta$ with grey regions indicating no secondary peak satisfying the threshold size within a period of five years (see the Methods). In (c) the times series of primary (solid lines) and secondary (dashed lines) infections are shown for various values of ϵ and a duration of immunity of $1/\delta = 1$ year. In (d) the times series of the fully susceptible (S_P, solid lines), immune (R, dashed lines), and partially immune (S_S, dotted lines) populations are shown for various values of ϵ and a duration of immunity of $1/\delta = 1$ year.

S3.4 Effect of vaccination on timing and magnitude of subsequent peaks

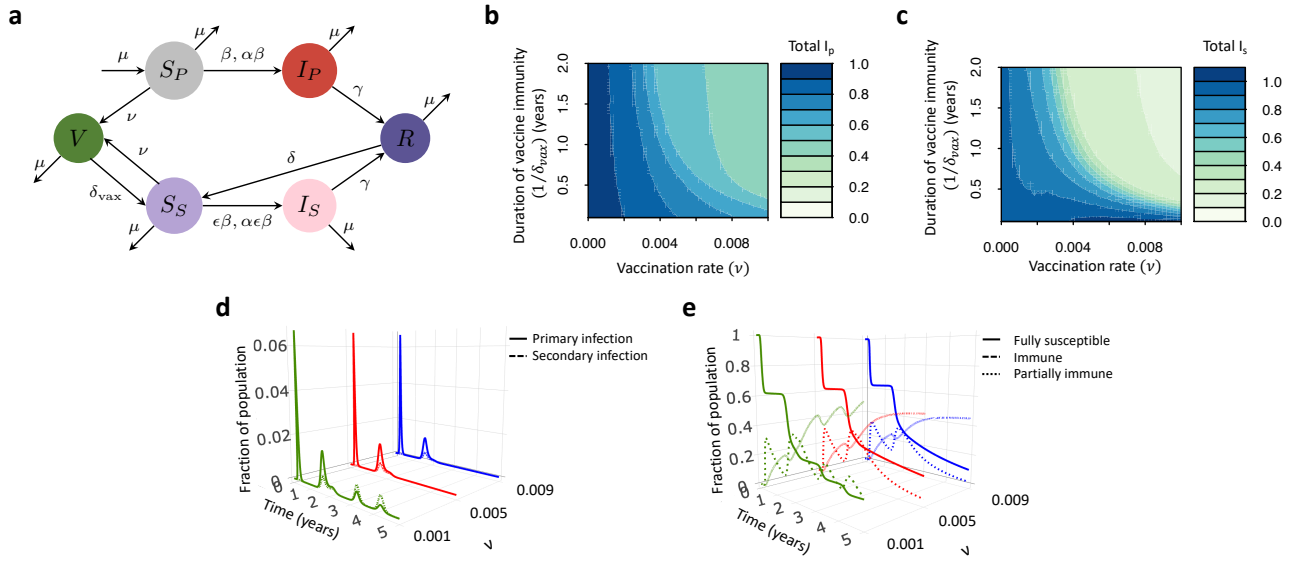

Figure S11: (a) Modified model flowchart that incorporates vaccination. In (b) and (c), the ratio of the total number of primary (b) and secondary (c) infections with vaccination versus without during years 1.5-5 inclusive (i.e. after the introduction of the vaccine) are plotted as a function of the weekly vaccination rate ν and the duration of vaccine immunity $1/\delta_{\text{vax}}$. In (d) and (e), time series of the various immune classes are plotted for different values of the vaccination rate ν. (d) contains the time series of primary (solid lines) and secondary (dashed lines) infections, while (e) contains the time series of the fully susceptible (solid lines), immune (dashed lines), and partially immune (dotted lines) subpopulations. The duration of vaccine immunity is taken to be $1/\delta_{\text{vax}} = 2$ years (longer than natural immunity). In (b) - (e), the susceptibility to secondary infection, relative transmissibility of secondary infections, and duration of natural immunity are taken to be $\epsilon = 0.7$, $\alpha = 1$, and $1/\delta = 1$ year, respectively. Vaccination is introduced 1.5 years after the onset of the epidemic following a 40 week period of social distancing during which the force of infection was reduced to 60% of its original value during weeks 16 to 55 (i.e. the scenario described in Figure 2b of the main text), and a seasonal transmission rate derived from the climate of NYC with no lag is assumed.

S3.5 Immune landscapes with pulse vaccination

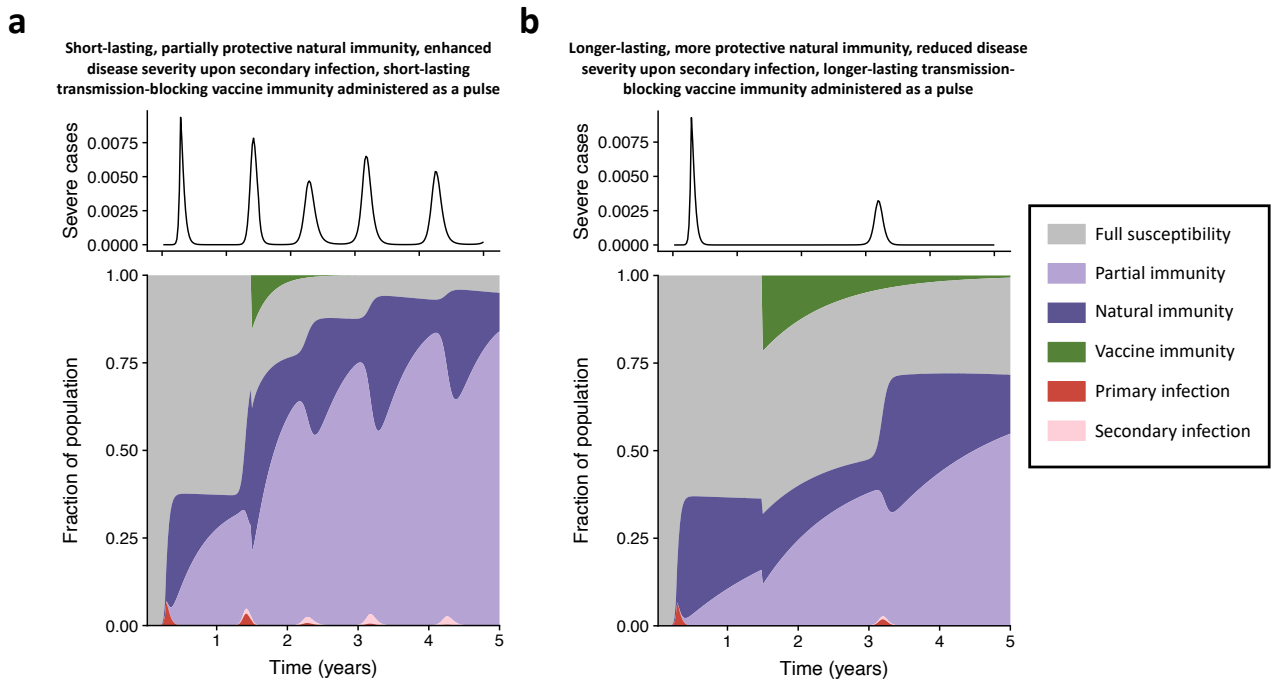

Figure S12: Time series of fraction of the population with severe cases I_{sev} (top) and area plots of the fraction of the population comprising each immune class (bottom) over a five year time period. In both plots, the relative transmissibility of secondary infections is taken to be $\alpha = 1$, a seasonal transmission rate derived from the climate of NYC with no lag is assumed, and a period of social distancing during which the force of infection is reduced to 60% of its original value during weeks 16 to 55 (i.e. the scenario described in Figure 2b of the main text) is enforced. Vaccination is introduced as a pulse in which 27% of the fully and partially susceptible populations are vaccinated with a transmission-blocking vaccine at $t_{\text{vax}} = 1.5$ years after the onset of the epidemic. (a) Corresponds to all the same parameters as in Figure 3a of the main text along with vaccine immunity lasting $1/\delta_{\text{vax}} = 0.25$ years, while (b) corresponds to all the same parameters as in Figure 3b of the main text along with vaccine immunity lasting $1/\delta_{\text{vax}} = 1$ year.

References

[1] S. E. Morris, V. E. Pitzer, C. Viboud, C. J. E. Metcalf, O. N. Bjørnstad, and B. T. Grenfell, "Demographic buffering: Titrating the effects of birth rate and imperfect immunity on epidemic dynamics," *Journal of the Royal Society Interface*, vol. 12, no. 104, 2015, ISSN: 17425662. DOI: 10.1098/rsif.2014.1245.

[2] M. Kissler, C. Tedijanto, E. Goldstein, Y. H. Grad, and M. Lipsitch, "Projecting the transmission dynamics of SARS-CoV-2 through the postpandemic period," *Science*, vol. In press, 2020.

[3] R. E. Baker, W. Yang, G. A. Vecchi, C. J. E. Metcalf, and B. T. Grenfell, "Susceptible supply limits the role of climate in the early sars-cov-2 pandemic," *Science*, 2020, ISSN: 0036-8075. DOI: 10.1126/science.abc2535. eprint: https://science.sciencemag.

org/content/early/2020/05/15/science.abc2535.full.pdf. [Online]. Available: https://science.sciencemag.org/content/early/2020/05/15/science.abc2535.

[4] J. Zhang, M. Litvinova, W. Wang, Y. Wang, X. Deng, X. Chen, M. Li, W. Zheng, L. Yi, X. Chen, Q. Wu, Y. Liang, X. Wang, J. Yang, K. Sun, I. M. Longini, M. E. Halloran, P. Wu, B. J. Cowling, S. Merler, C. Viboud, A. Vespignani, M. Ajelli, and H. Yu, "Evolving epidemiology and transmission dynamics of coronavirus disease 2019 outside Hubei province, China: a descriptive and modelling study," *The Lancet Infectious Diseases*, vol. 3099, no. 20, pp. 1–10, 2020, ISSN: 14744457. DOI: 10.1016/S1473-3099(20)30230-9. [Online]. Available: http://dx.doi.org/10.1016/S1473-3099(20)30230-9.

[5] R. Gelaro, W. McCarty, M. J. Suárez, R. Todling, A. Molod, L. Takacs, C. A. Randles, A. Darmenov, M. G. Bosilovich, R. Reichle, *et al.*, "The modern-era retrospective analysis for research and applications, version 2 (merra-2)," *Journal of Climate*, vol. 30, no. 14, pp. 5419–5454, 2017.

[6] R Core Team, *R: A language and environment for statistical computing*, R Foundation for Statistical Computing, Vienna, Austria, 2013. [Online]. Available: http://www.R-project.org/.

[7] Z. Wu and J. M. McGoogan, "Characteristics of and important lessons from the coronavirus disease 2019 (COVID-19) outbreak in China: Summary of a report of 72314 cases from the Chinese Center for Disease Control and Prevention," *JAMA*, vol. 323, no. 13, pp. 1239–1242, 2020, ISSN: 15383598. DOI: 10.1001/jama.2020.2648.

[8] W. J. Guan, Z. Ni, Y. Hu, W. Liang, C. Ou, J. He, L. Liu, H. Shan, C. L. Lei, D. S. Hui, B. Du, L. J. Li, G. Zeng, K. Y. Yuen, R. C. Chen, C. L. Tang, T. Wang, P. Y. Chen, J. Xiang, S. Y. Li, J. L. Wang, Z. J. Liang, Y. X. Peng, L. Wei, Y. Liu, Y. H. Hu, P. Peng, J. M. Wang, J. Y. Liu, Z. Chen, G. Li, Z. J. Zheng, S. Q. Qiu, J. Luo, C. J. Ye, S. Y. Zhu, and N. Zhong, "Clinical characteristics of coronavirus disease 2019 in China," *The New England Journal of Medicine*, vol. 382, no. 18, pp. 1708–1720, 2020, ISSN: 15334406. DOI: 10.1056/NEJMoa2002032.

[9] J. Zhang, M. Litvinova, Y. Liang, Y. Wang, W. Wang, S. Zhao, Q. Wu, C. Viboud, A. Vespignani, M. Ajelli, and H. Yu, "Changes in contact patterns shape the dynamics of the COVID-19 outbreak in China," *Science*, vol. In press, 2020.

[10] T. Britton, F. Ball, and P. Trapman, "A mathematical model reveals the influence of population heterogeneity on herd immunity to sars-cov-2," *Science*, 2020, ISSN: 0036-

8075. DOI: 10.1126/science.abc6810. eprint: https://science.sciencemag.org/content/early/2020/06/22/science.abc6810.full.pdf. [Online]. Available: https://science.sciencemag.org/content/early/2020/06/22/science.abc6810.

[11] A. A. King, S. Shrestha, E. T. Harvill, and O. N. Bjørnstad, "Evolution of acute infections and the invasion-persistence trade-off," *The American Naturalist*, vol. 173, no. 4, pp. 446–455, 2009, ISSN: 15378276. DOI: 10.1038/jid.2014.371. arXiv: NIHMS150003. [Online]. Available: https://www.ncbi.nlm.nih.gov/pmc/articles/PMC3624763/pdf/nihms412728.pdf.

[12] Q.-X. Long, X.-J. Tang, Q.-L. Shi, Q. Li, H.-J. Deng, J. Yuan, J.-L. Hu, W. Xu, Y. Zhang, F.-J. Lv, K. Su, F. Zhang, J. Gong, B. Wu, X.-M. Liu, J.-J. Li, J.-F. Qiu, J. Chen, and A.-L. Huang, "Clinical and immunological assessment of asymptomatic SARS-CoV-2 infections," *Nature Medicine*, pp. 1–5, 2020, ISSN: 1078-8956. DOI: 10.1038/s41591-020-0965-6. [Online]. Available: http://www.nature.com/articles/s41591-020-0965-6.